Spectral Characteristics of Tapered LPG Device as a Sensing Element for Refractive Index and Temperature

T. Allsop, F. Floreani, K. P. Jedrzejewski, P. V. S. Marques, R. Romero, D. J. Webb, *Member, IEEE*, and I. Bennion

***Abstract*—The fabrication and characterization of long-period gratings (LPGs) in fiber tapers is presented alongside supporting theory. The devices possess a high sensitivity to the index of aqueous solutions due to an observed spectral bifurcation effect, yielding a limiting index resolution of $\pm 8.5 \times 10^{-5}$ for solutions with an index in the range 1.330–1.335.**

***Index Terms*—Long-period fiber gratings, optical fiber devices, optical fiber tapers, refractive-index measurement, temperature measurement.**

I. Introduction

LONG-PERIOD gratings (LPGs) and both adiabatic and nonadiabatic tapers in fibers are all devices that couple light from the fiber core into cladding modes. An LPG is an axially periodic refractive-index variation inscribed in the core of a photosensitive single-mode optical fiber by ultraviolet (UV) radiation or other means, which couples light from the core to cladding modes at discrete wavelengths [1], [2]. In a fiber taper, it is the change of the waveguide radius that enables coupling between the modes [3], producing applications in chemical/biological and strain sensing [4], [5]. The study of LPGs has yielded many potential uses in the area of telecommunications and numerous sensing applications. This is because the mean wavelengths of the attenuation bands are susceptible to strain, temperature, curvature, and the refractive index of the surrounding medium [1], [2], [6], [7]. In particular, there has been strong interest in using LPGs as chemical sensors [6], [7], for example, in the detection of organic aromatic compounds in paraffin [7]. Recently, there has been some interest in combining both types of fiber sensors for chemical sensing [8], [9], leading to high-resolution index measurements.

We report for the first time the new spectral behavior of LPGs recorded in fiber tapers and propose a suitable mechanism responsible for this behavior. These tapered-fiber LPG devices have a high sensitivity to refractive indexes around 1.3, which suggests that they may be especially suitable for refractive-index monitoring of aqueous solutions.

Manuscript received March 24, 2005; revised August 16, 2005.

T. Allsop, F. Floreani, D. J. Webb, and I. Bennion are with the Photonics Research Group, Aston University, Birmingham, B4 7ET, U.K. (e-mail: t.d.p.allsop@aston.ac.uk; floreanf@aston.ac.uk; d.j.webb@aston.ac.uk; I.Bennion@aston.ac.uk).

K. P. Jedrzejewski is with the Institute of Electronic Systems, Warsaw University of Technology, Warsaw 00-665, Poland (e-mail: Kpj@ise.pw.edu.pl).

P. V. S. Marques and R. Romero are with the INESC Porto, Unidade de Optoelectrónica a Sistemas Electrónicos, Porto 4169-007, Portugal (e-mail: psmarque@fc.up.pt; rosa.muniz@fc.up.pt).

Digital Object Identifier 10.1109/JLT.2005.862426

II. Theory

In the modeling of these fiber devices, two fundamental mechanisms have to be considered. First, the taper geometry itself is important. The coupling from the core mode to the local taper cladding modes can be investigated by using the slowness criterion [10] to determine whether the fiber taper is adiabatic or nonadiabatic. In addition, the evolution of the core mode itself along the length of the taper can be scrutinized by means of the V parameter of the fiber, which determines the radius at which the core-to-cladding-mode transition takes place [11]. Second, the coupling to the local cladding modes by the LPG itself must also be taken into account, which involves determining how the phase-matching conditions and the coupling constants vary along the fiber device. Again, the same mechanisms have to be considered when the fiber device is subjected to environmental changes such as temperature, bending, and changes in refractive index of the surrounding medium.

A. Modeling of the Fiber Taper

In order to maintain adiabaticity, and thus have negligible coupling between modes, the magnitude of the gradient of the radius of the fiber along the taper should be significantly smaller than the adiabatic length scale [12]; otherwise, strong mode coupling is to be expected [10], [12]. This condition is given by the slowness criterion [10]

$$\left|\frac{\partial r}{\partial z}\right| \ll \frac{r}{z_{\mathrm{b}}}, \qquad \text{with } z_{\mathrm{b}} = \frac{2\pi}{\beta_1 - \beta_2}. \tag{1}$$

Here, z_{b} is the beat length between two modes with propagation constants β_1 and β_2, r is the radius of the fiber along the taper, and r/z_{b} is the adiabatic length-scale criteria. To determine where this condition was met, the shapes of the tapered optical fibers used were measured using a microscope imaging system (Axioskop, Zeiss).

The fiber tapers were analyzed in a stepwise method reflecting the rate of radius variation: A taper was divided into a series of sections for which the local modes were calculated. For each section of the tapered fiber, the modes were evaluated

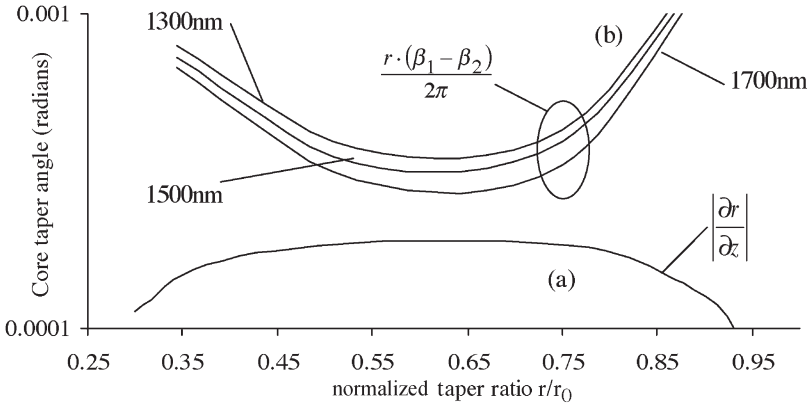

Fig. 1. (a) Modulus of the slope profile of a typical biconical taper used in these investigations. (b) Calculated slowness-criterion limit curves for three wavelengths for the same typical biconical taper.

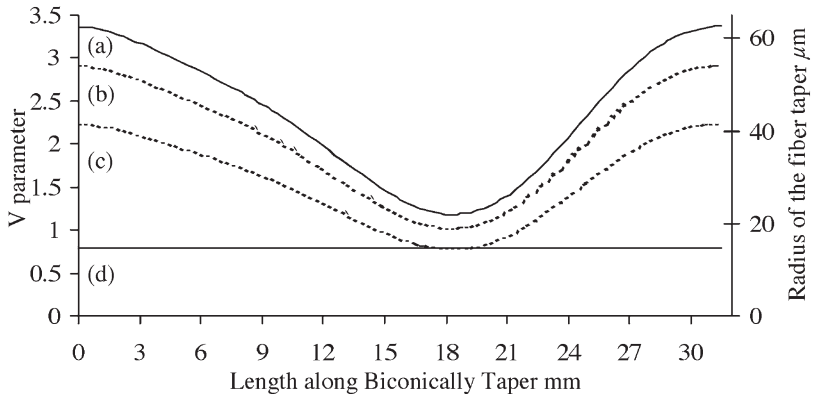

Fig. 2. Some of the physical characteristics of a typical fiber taper used in this investigation (as used for Fig. 1). (a) Variation of the radius of the taper along its length. (b) V-number variation of the taper at 1300 nm. (c) V-number variation of the taper at 1700 nm. (d) Core-mode cutoff value.

by obtaining the values of the core and cladding modes' effective $(n_{\rm co}^{01}, n_{\rm cl}^{\nu})$ and group $(n_{\rm cog}, n_{{\rm clg}_\nu})$ indexes. In addition, the respective propagation constants β_ν were obtained by numerically solving the dispersion relationship for a three-layered fiber using the technique described by Erdogan [13]. The predicted values were confirmed using Tsao's expressions [14].

Using the numerical results obtained with the measured radius profile of the tapered fiber, it was found that these tapers are adiabatic, and thus, negligible coupling occurs between the core and the cladding modes (see Fig. 1). Next, the V parameter of the fiber core needs to be considered. The V parameter decreases due to the reduction of the core radius, leading to an increase of the core-mode field diameter, which finally extends through the cladding. At this point, the light is no longer guided by the core–cladding interface but is guided by the cladding–external medium interface, thus becoming the $\rm HE_{1,1}$ mode of the cladding. The condition for this core-mode cutoff is reached when the V number of the core and the ratio S of the cladding diameter to the core diameter match as follows [11]:

$$V_{\rm Core} \cong \sqrt{\frac{2}{\ln S + 0.26}}. \tag{2}$$

For any smaller fiber radii beyond this point, no LPG-induced mode coupling takes place. This is due to the fact that the effective overlap of the electric fields between modes decreases with the transverse area of the index perturbation and because the fundamental core mode no longer exists. Therefore, for this adiabatic fiber taper, over the length where the core-mode cutoff exists, there is no interaction between the $\rm HE_{1,1}$ mode and other modes. The variation of the taper's radius and the V number along the taper length is shown in Fig. 2, along with the core-mode cutoff value.

B. Modeling of the Fiber LPG

The LPG couples incident light to the forward-propagating cladding modes of the optical fiber, which decay through radiation. The fiber supports many cladding modes, each potentially corresponding to an attenuation band in the LPG transmission spectrum. The center wavelength λ_ν of an attenuation band is specified by the phase-matching condition

$$\delta n_{{\rm eff}_\nu} \Lambda = \lambda_\nu \tag{3}$$

where

$$\delta n_{{\rm eff}_\nu} = \left[n_{\rm co}^{01}(\lambda, \varepsilon, T, n_1, n_2) - n_{\rm cl}^{1\nu}(\lambda, \varepsilon, n_1, n_2, n_{\rm s}, T)\right] \tag{4}$$

$n_{\rm co}^{01}$ is the effective index of the core mode, and $n_{\rm cl}^{1\nu}$ the effective index of the νth radial cladding mode, both indexes being

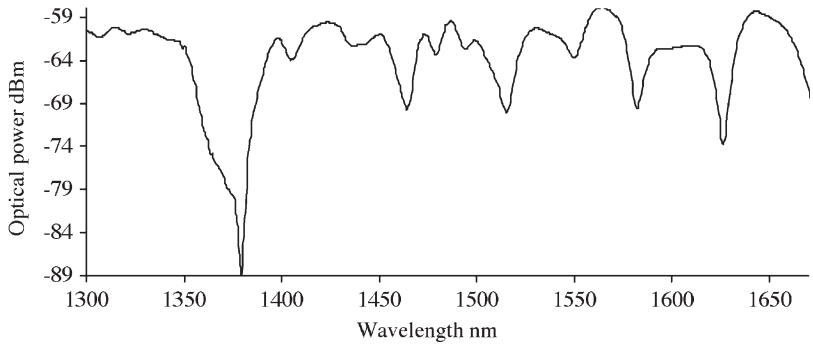

Fig. 3. Transmission spectrum of a tapered LPG fiber device with a period of 350 μm.

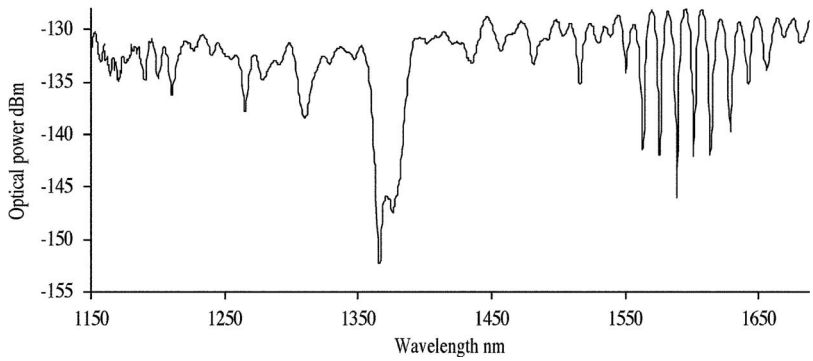

Fig. 4. Transmission spectrum of a tapered LPG fiber device with a period of 500 μm.

dependent on the core refractive index n_1, the cladding refractive index n_2, and the wavelength λ. Also, $n_{\rm cl}^{1\nu}$ is a function of the refractive index $n_{\rm s}$ of the surrounding medium. Λ is the period of the LPG, T the temperature, and ε the strain experienced by the fiber. The quantity $\delta n_{{\rm eff}_\nu}$ is the differential effective index between the core and cladding modes. In (4), the superscripts denote the $\rm LP_{01}$ core mode and the $\rm HE_{1\nu}$ axially symmetric cladding modes: From this point forward, we replace 1ν with ν. We are assuming here that the grating consists of a circularly symmetric index perturbation transverse to the axis of the fiber, so that the only nonzero coupling coefficients between the core mode and the cladding modes involve cladding modes of azimuthal order 1 [13]. The properties of the individual cladding modes may be observed through their associated attenuation bands. Equations (3) and (4) are used to give the local cladding modes' phase-matching conditions along the tapered fiber.

III. Fabrication of the Tapered LPG Devices

The biconical tapers were fabricated using single-mode standard communications step-index optical fiber with an initial core radius of 4.5 μm and with an outer cladding radius of 62.5 μm. The tapers themselves were produced by applying a controlled tension to the fibers while they were subjected to a flame in one case [15] or to an electric arc in the second case [16]. Presented here are devices in tapers with a total length of 3.2 cm and minimum waist radii down to 25 μm fabricated with the former method. Photosensitivity in the fibers was increased by hydrogenation at a pressure of 120 bar over a period of two weeks at room temperature. The uniform standard LPGs were fabricated using a frequency-doubled argon ion laser with a point-by-point writing technique. The total length of all LPGs was 5 cm, with the central section of each LPG being inscribed into the fiber taper. A series of these LPG devices was fabricated at periods from 500 to 150 μm.

The characterization of the attenuation bands was carried out by observing the transmission spectrum with an optical spectrum analyzer (OSA), with a resolution of 1 nm, when the LPG was illuminated by a broadband light source. Two typical transmission spectra of these devices are shown in Figs. 3 and 4.

LPGs with periods from 500 to 250 μm, written in fiber tapers fabricated using both taper drawing methods, showed similar spectral features of comparable strength and included discrete attenuation bands and/or a Mach–Zehnder-like interference effect (see Fig. 4 in the region of 1600 nm). The presence of both kinds of spectral features in the transmission spectra of these devices (such as that shown in Fig. 4) can be explained by considering the V number along the taper's length at different wavelengths. These tapers have radii of approximately 25 μm, which is close to the core-mode cutoff value (see Fig. 2); thus, in some cases, at the longer wavelengths (as seen in Fig. 4 at $\sim$ 1600 nm), the core-mode cutoff V number is achieved. Other devices showed no Mach–Zehnder-like effect due to the fact that the V numbers for all measured wavelengths were greater than the core-mode cutoff V number. At the lower periods (250–150 μm) used for the devices, the discrete bands were less pronounced, and no Mach–Zehnder effect was observed over the wavelength range measured. A possible explanation for

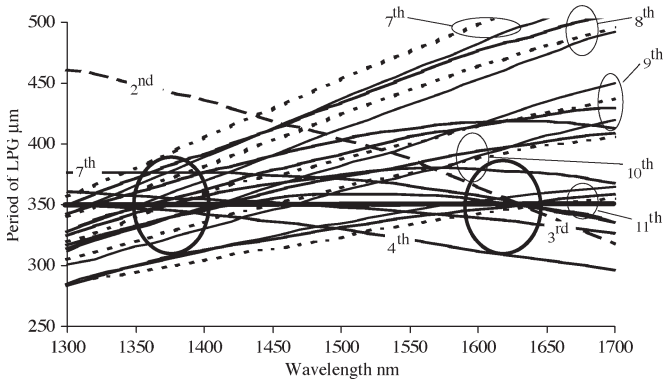

Fig. 5. Phase-matching curves for cladding modes (labeled) associated with various radii along the fiber taper: 62.5 μm, 58.9 μm, 54.2 μm, 49.7 μm, 40.1 μm, 33.9 μm, and 28.0 μm. The horizontal line corresponds to the experimentally used grating period (350 μm).

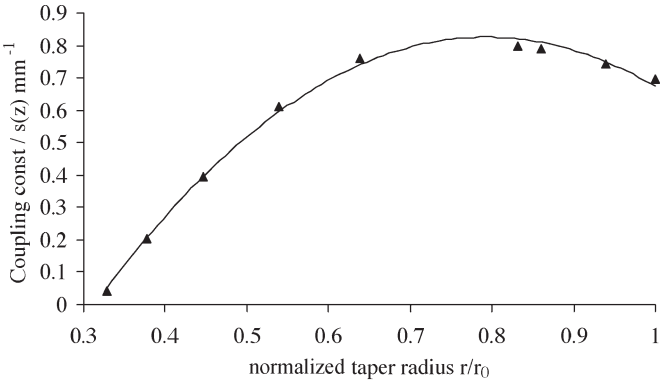

Fig. 6. Variation in the strength of the coupling constant between the core mode and the $HE_{1,9}$ local cladding mode as a function of normalized radius of the fiber taper.

these features is that attenuation bands associated with higher order cladding modes tend to have smaller coupling constants [13] and generate less pronounced spectral features.

The Mach–Zehnder-like spectral feature can be explained by calculating the V number using (2), which yields a core-mode cutoff at radii of about 25 μm or below, which corresponds to about 6 mm of the total length of the fiber taper used with the LPG with a period of 500 μm. As explained earlier, in this section of the adiabatic fiber taper, there is negligible LPG-induced coupling, and this section forms an effective cavity between the two outer sections of the LPG. This effect has been reported elsewhere in ordinary fiber [10].

We propose that the discrete spectral features present in the transmission spectra of the LPG devices (shown in Figs. 3 and 4) can be explained in two parts; this is supported by a theoretical study of these devices and some experimental evidence. The first part of the explanation is derived from the modeling of the tapered LPG and the second from measurements of the refractive index and temperature spectral sensitivities of these devices along with observations made during the UV inscription of the LPGs.

First, we consider the theoretical phase-matching conditions of the local cladding modes. The phase-matching conditions were calculated for various sections of the taper using the slowness criteria to determine the length of each section of the taper. The lengths were chosen to ensure that the E fields do not significantly change their phase along the fiber section [10] compared to light guided in a nontapered fiber of the same initial diameter. This approach yielded the phase-matching conditions for various local cladding modes along sections of the taper. From Fig. 5, it can be seen that various local modes of different sections of the taper have the same phase-matching conditions at roughly the same spectral locations (circled in the figure).

It can be seen in Fig. 5 that for an LPG with a period of 350 μm, there are several local cladding modes' attenuation bands having approximately the same spectral locations, which coincide with the main spectral features in Fig. 3 at $\sim$ 1350 and $\sim$ 1650 nm (circled in Fig. 5). Also, the smaller spectral features that appear in the transmission spectra at $\sim$ 1450 nm and $\sim$ 1500 m are approximately phase matched to other cladding modes shown in the figure. The small variation in the phase-matching condition for various modes will generate attenuation bands that overlap and appear as a single wide attenuation band in the transmission spectrum of the LPG device, which partly explains the broadness of the experimentally observed features. A typical 3-dB bandwidth for an LPG (uniform, length of 5 cm, period of 350 μm) written in standard telecomm fiber is $\sim$ 7 nm, compared to the $\sim$ 50- to $\sim$ 60-nm bandwidths of the main spectral features in the tapered LPG device with a period of 350 μm.

Second, to obtain a better understanding of the discrete features present in the transmission spectrum of these devices, the coupling constants for the local cladding modes for each section along the tapered LPG were calculated. The coupling constants are calculated by the procedure described by Erdogan [13]. Fig. 6 shows the variation of the coupling constant for the $HE_{1,9}$ local mode, which is a typical cladding mode, as a function of the radius of the fiber, assuming that the core radius changes by the same factor as that of the cladding. The behavior of the coupling constant arises due to the fact that the taper profile affects the coupling coefficients for the core to cladding modes as a function of the radius along the taper length [17].

This offers an explanation as to why discrete spectral features are still present in the transmission spectra of the tapered LPG device. Along the taper length, the LPG's coupling strength decreases, while the phase-matching condition changes simultaneously. The resultant attenuation bands will broaden but still be discrete because in the center of the taper, the coupling coefficients become significantly smaller compared to other sections along the taper length.

Some experimental evidence for this proposed mechanism was observed during postfabrication UV exposure of one tapered LPG fiber device. After the LPG inscription, the midsection of the taper, measuring 4 mm, was exposed to uniform UV light sufficient to saturate the photosensitivity of the fiber; this resulted in no noticeable change of the transmission spectrum. This observation suggests that there is negligible coupling occurring in the midsection of the taper, which is consistent with the predictions of Fig. 6.

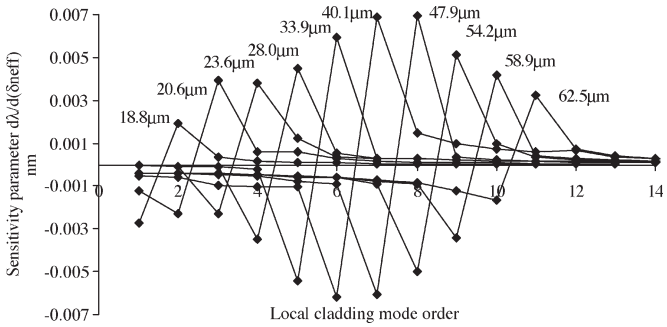

Fig. 7. Spectral-sensitivity parameter at a wavelength of 1500 nm for sections of the tapered LPG with different radii, as shown in the figure.

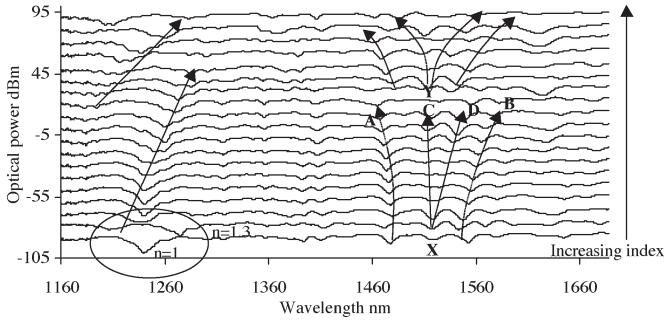

Fig. 8. Transmission spectrum of a tapered LPG fiber device with a period of 400 μm when the refractive index is changed between 1.00 and 1.37.

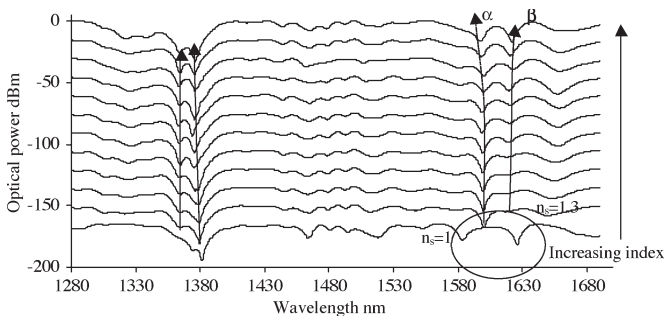

Fig. 9. Transmission spectrum of a tapered LPG fiber device with a period of 350 μm when the refractive index is changed between 1.00 and 1.36.

Other evidence of this mechanism can be obtained from considering the general sensitivity parameter of the LPG [2] in conjunction with the experimental results shown in the next sections. A general sensitivity parameter can be calculated from [2], which is relevant to each of the measurands and contributes to the spectral sensitivity of the device as a function of cladding-mode order. The general sensitivity parameter is dependent upon the difference between the differential effective index and the differential group index and includes the wavelength dependence [2]

$$\left(\frac{d\lambda}{d\delta n_{\text{eff}}}\right)_{\nu} = \frac{\lambda}{(\delta n_{\text{eff}_{\nu}} - \delta n_{g_{\nu}})}. \tag{5}$$

This parameter depends on the gradient of the $\Lambda-\lambda$ curves [1]. As may be seen from Fig. 5, the slopes of these curves can have either sign, depending on the particular cladding mode and fiber radius; consequently, the different cladding modes have very different sensitivities along the fiber taper. This is brought out further in Fig. 7, where we have used the procedure described previously to obtain the effective $(n_{\text{co}}^{01}, n_{\text{cl}}^{\nu})$ and group $(n_{\text{cog}}, n_{\text{clg}_{\nu}})$ indexes, and the sensitivity parameter for each section of the tapered LPG was calculated (see Fig. 7). In the later sections, this phenomenon is investigated further with respect to temperature sensitivity and exploited to measure refractive index.

This figure shows that at a given wavelength, local cladding modes and their associated attenuation bands exhibit both blue and red wavelength shifts, depending on the position along the taper. The sensitivity of the device is increased at those locations along the taper where the LPG couples to a local cladding mode at its "turning point" of sensitivity [2]. In general, in a standard fiber, the "turning point" can exist for only one cladding mode at a given wavelength.

IV. Refractive-Index Sensitivity of the Tapered LPG Fiber Device

For refractive-index-sensitivity measurements, the LPG device was placed in a V groove and immersed in certified refractive index (CRI) liquids (supplied by Cargille Laboratories Inc.) that have a quoted accuracy of ± 0.0002. The LPG device and V groove were carefully cleaned, washed in methanol, then in deionized water, and finally, dried before the immersion of the LPG device into a CRI liquid. The V groove was machined into an aluminum plate, to minimize bending of the fiber. The plate was placed on an optical table that acted as a heat sink to maintain a constant temperature. The typical spectral responses of two LPGs to changes in the refractive index are shown in Figs. 8 and 9.

The spectral refractive-index sensitivity of the features labeled **A** and **B** of the 400-μm-period grating are shown in Fig. 10(a), and the sensitivity of the spectral features labeled $\boldsymbol{\alpha}$ and $\boldsymbol{\beta}$ of the 350-μm-period grating are shown in Fig. 10(b). Inspecting the transmission spectra in Figs. 8 and 9, it can be seen that there are two effects of interest in the evolutionary spectral behavior.

First, both figures exhibit a spectral feature that splits and separates. This "bifurcation" effect gives rise to individual features that evolve with either a blue or red wavelength shift as a function of refractive index [features such as **A**, **B**, **C**, and **D**, evolving from spectral location **X** or **Y** (seen in Fig. 8), and $\boldsymbol{\alpha}$ and $\boldsymbol{\beta}$ (seen in Fig. 9)] in the absence of any evidence of induced birefringence. These experimental results in conjunction with consideration of the spectral-sensitivity parameter (Fig. 7) suggest that there are spectrally matched and overlapping attenuation bands present in the transmission spectra of these devices.

Second, the circled spectral features in Figs. 8 and 9 show dramatic changes from indexes of 1 to 1.3, suggesting that these devices may be useful for the detection of substances that have a low refractive index.

The refractive-index spectral sensitivity was calculated using the procedure adopted by Allsop *et al.* [2] and gives the

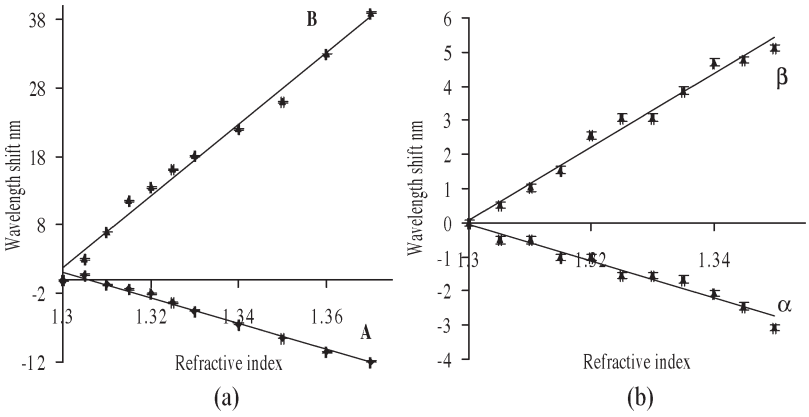

Fig. 10. Spectral sensitivity of selected spectral features as a function of refractive index for (a) 400-μm-period LPG device and (b) 350-μm-period LPG device.

maximum value of the sensitivity as the mode becomes unguided, given by

$$\left(\frac{d\lambda}{dn_{\rm s}}\right)_{\nu} = \left(\frac{d\lambda}{d\delta n_{\rm eff}}\right) \cdot \left(-\left[\frac{n_{\rm s}}{n_{\rm cl}^{\nu}}\right] \cdot \left(\frac{U_{*_\nu}}{\upsilon_\nu}\right)^2 \cdot \left[1 + \left(\frac{\upsilon_\nu}{2}\right) \cdot \frac{U_\infty(\nu)^2}{(1+\upsilon_\nu)^3}\right]\right) \quad (6)$$

where $\upsilon_\nu^2 = u_k^2 + u_{k+1}^2$, u_k and u_{k+1} are the phase parameters for consecutive cladding layers of the optical fiber, and n_k is the refractive index of the kth layer. The maximum value of $k+1$ is 3, denoting the medium surrounding the fiber. Also, the phase parameter must be real for the mode to be guided within the fiber. $U_\infty(\nu)$ is the value taken by u when υ (the normalized frequency) becomes infinite for the νth mode [18]. U_* is the approximate expression for the phase parameter u_ν, obtained from the characteristic equation of a fiber waveguide for large υ, developed by Miyagi *et al.* [18]. Using (6), we obtained the spectral sensitivity of the attenuation bands for the first radially symmetric cladding modes (see Fig. 11).

A general observation of this type of LPG sensor is that it exhibits a higher spectral sensitivity to the surrounding medium's refractive index in the range of 1.300–1.340 than either a single LPG in a standard optical fiber or a Mach–Zehnder LPG (MZLPG) [19]. The maximum measured spectral sensitivity of the tapered LPG devices was obtained with a period of 400 μm, which gave experimentally $d\lambda/dn = +713$ nm (wavelength difference between **A** and **B**), as shown in Fig. 10(a), which is also greater than reported values in other fiber LPG devices such as those recorded in a step-index fiber, where $d\lambda/dn = +324$ nm has been measured, or in a W-index-profile fiber, where $d\lambda/dn = -318$ nm has been reported [2].

The increase in the sensitivity for surrounding media with a refractive index in the region of that of water $(n = 1.333)$ is significant, which enables measurements of aqueous solutions with high accuracy. Also, the maximum overall wavelength shifts for indexes from 1 to 1.300 were significantly greater for these devices than any conventional LPG devices. A comparison of the values is presented in Table I.

To assess their performance with aqueous solutions, the sensitivity of the tapered LPGs was further investigated using saline (NaCl) solutions. An MZLPG was used to calibrate the index of the solutions in the spectral region of interest. First, an MZLPG was calibrated with the CRI liquids. Then, the calibrated MZLPG was placed in a bath containing 500 ml deionized water and a 2-molar solution of NaCl was added to and stirred in this water in increments of 10 ml. The water used for this investigation came from a single container, which had the same ambient temperature as the room where the experiment was carried out. The temperature of the solution was monitored and held constant at 0.1 °C. The devices were illuminated with a broadband light source and an OSA with a resolution of 0.1 nm was used to monitor the wavelength shifts during the experiments (see Fig. 12).

Comparing these wavelength shifts with the wavelength shifts obtained from the CRI liquids, and assuming linearity, allowed us to determine the average increase in the refractive index per increment of 10 cc of 2-molar NaCl solution to the 500 cc of deionized water. The addition of the 10-cc NaCl solution gave an increase in refractive index of $(3.2 \pm 0.7) \times 10^{-4}$. The same experiment was repeated with the tapered LPG device (period of 400 μm, length of 5 cm), and the results are shown in Fig. 13(a) and (b).

We considered two ranges around 1.330 and 1.335, the first range yielding a sensitivity of $d\lambda/dn = 1500 \pm 36$ nm, which leads to a limiting resolution of $\pm 8.5 \times 10^{-5}$ for the present scheme. The second range (near 1.335) yields a sensitivity of $d\lambda/dn = 560 \pm 55$ nm, which leads to a limiting resolution of $\pm 3.3 \times 10^{-4}$. The uncertainty in the CRI liquids limits the present accuracy to that of the calibration liquids themselves.

V. Temperature Sensitivity of the Tapered LPG Fiber Device

The experimental apparatus for measuring the temperature sensitivity of the LPGs is similar to the one for $n_{\rm s}$. Instead of the LPG being immersed in the liquids, it was placed on the top of an insulated Peltier cooler. The temperature was varied

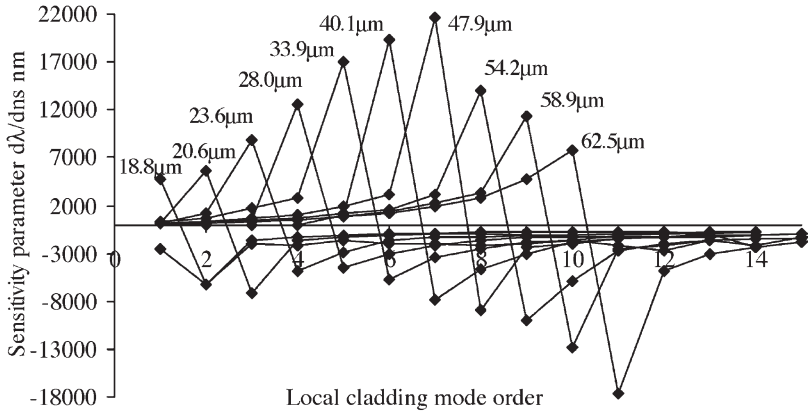

Fig. 11. Theoretical predictions for spectral sensitivity for the tapered LPG fiber as a function of the surrounding medium's refractive index at a wavelength of 1500 nm for sections of the fiber-tapered LPG device with different radii, as shown in the figure.

TABLE I
COMPARISON OF LPG FIBER DEVICES

The type of wavegiude the long period grating is written into	Maximum Total wavelength shifts for a main feature for surrounding index from 1.0 to 1.300	Typical absolute wavelength shifts for a main feature for surrounding index from 1.0 to 1.300	Maximum spectral sensitivity for a main feature of the device for surrounding index 1.333	Typical absolute spectral sensitive for a main feature of the device for surrounding index 1.333
	nm	nm	dλ/dns	dλ/dns
Step-Index fiber [a]	−16nm to +14nm	7nm	324nm	100nm
W-profile fiber [b]	−14nm to −3nm	3nm	−318nm	80nm
Step-Index fiber Tapers	+68nm to −21nm	40nm	713nm	400nm

[a] data from reference 2
[b] data from reference 2

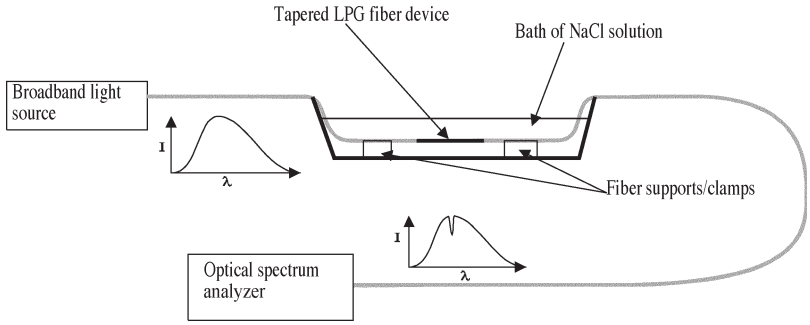

Fig. 12. Schematic of the experiment for salinity measurement.

and the wavelength shift of the attenuation bands of each LPG measured. Some typical results are shown in Fig. 14.

The temperature sensitivity $(d\lambda/dT)$ of the 400-μm-period LPG device varied from $+0.087$ to -0.022 nm°C^{-1}, suggesting again that several overlapping attenuation bands exist. The other tapered LPG fiber devices were also investigated and showed similar results. The spectral temperature sensitivity of other tapered LPG fiber devices varied from $+0.12$ to -0.1 nm°C^{-1}, which is significantly lower than the highest temperature sensitivities recorded for conventional fiber LPG (~ 0.3 nm°C^{-1}). This difference in the sensitivity may be due to the different materials used for producing the fibers and the consequent variations in the difference between the thermo-optic coefficient of the core and cladding, which directly affects the sensitivity.

VI. DISCUSSION

While it is acknowledged by the authors that the given explanation for the bifurcation effect may be simplistic in its approach in view of the complexity of the LPG fiber device, the proposed mechanism is supported by a well-established waveguide and grating theory and by the experimental observations and data.

The comparison of these experimental results against other index-measuring systems is favorable. First, Abbe refractometers have resolutions of 10^{-4} down to 2×10^{-5} (1.33–1.58) and are relatively expensive, whereas this system has comparable or better resolution. It can be used remotely and has the potential for being low cost. Second, sensors have been demonstrated based on fiber Bragg grating (FBG) evanescent field interactions [20] that yield an index resolution of around 10^{-3} (1.3)

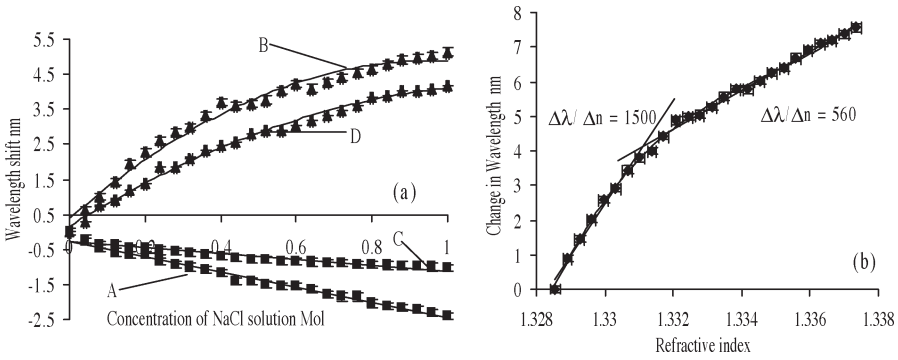

Fig. 13. (a) Spectral sensitivity and (b) variation of the wavelength separation of the spectral features **A** and **B** as a function of molar concentration of the NaCl solution.

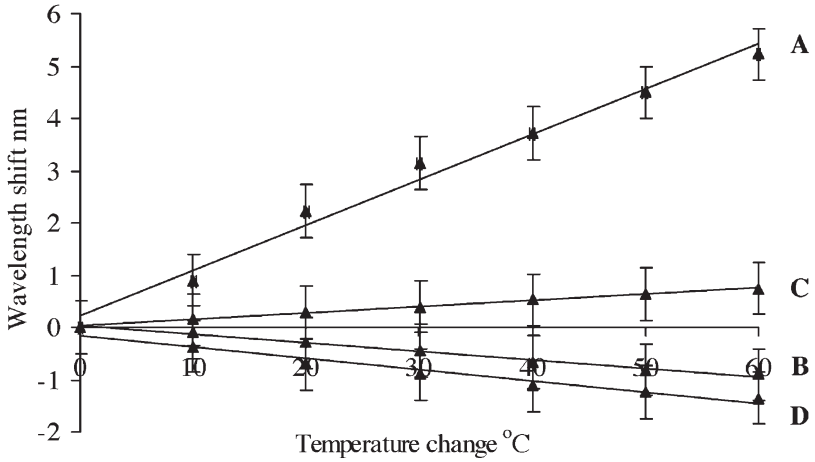

Fig. 14. Spectral sensitivity of the labeled spectral features of the tapered LPG fiber device with a period of 400 μm and a length of 5 cm.

but require a more complex optical arrangement. Third, LPG-based systems such as that in [7] are best used to investigate refractive indexes greater than 1.4, where the spectral sensitivity of the LPG is intrinsically greater.

Another interesting spectral property of these LPG devices is that some of their discrete spectral features exhibit dramatic changes in their transmission profile from indexes of 1 to 1.3, suggesting that they may be useful for the measurement of substances that have a low refractive index; this is the subject of current investigations.

VII. Conclusion

In view of the rather complicated behavior of the devices under study and the consequent complexity of our proposed explanation of the behavior, we feel it appropriate here to summarize the main aspects of the paper.

First, the fiber taper's spectral properties were considered with regard to adiabatic and nonadiabatic behavior along with the condition for core-mode cutoff. To assist in determining the behavior of the fiber tapers, their physical profiles were measured, and these measurements were used to calculate the variation of the V parameter along the fiber taper and, thus, the presence of core-mode cutoff. Determining the adiabaticity of the tapers was done by considering the slowness criteria, which first uses the profile measurements (the magnitude of the gradient of the radius of the fiber) and, second, the adiabatic length scale of the fiber tapers. The adiabatic length-scale calculations involved determining the propagation constants of the core and local cladding modes in a stepwise approach along the length of the taper. These considerations showed that the tapers were adiabatic and, for most of their length, were above the core-mode cutoff radius. It was possible to construct a series of $\Lambda-\lambda$ dispersion curves for the modes at various positions along the devices. This revealed that several local cladding modes had approximately the same phase-matching condition for the 400- and 350-μm-period devices, producing resonances at wavelengths where strong attenuation bands were observed experimentally. Also, the coupling constants for local modes along the device were calculated using the approach given in [13], from which it was found that coupling to the local cladding modes decreased significantly in the center of the taper where the phase-matching conditions changed appreciably, offering an explanation to the presence of broad, but still discrete, spectral features. Consideration of the general sensitivity parameter suggested that, in response to changes in temperature or surrounding refractive index, particular attenuation bands should have both blue and red shifts, depending on the position along the taper. This consideration is offered as an explanation of the blue and red shifts (bifurcation) observed within the fine structure of some attenuation bands.

In conclusion, for the first time, to the authors' knowledge, a new spectral bifurcation effect in fiber LPGs has been observed, and a suitable mechanism for its origin has been proposed, which is supported by experimental results. These devices have a greater spectral sensitivity with respect to refractive index in the 1.333 range than other fiber-grating sensors, which suggests that this device may be suitable for refractive-index monitoring of aqueous solutions.

REFERENCES

[1] S. Vasilev *et al.*, "Long-period refractive index fibre gratings: Properties, applications and fabrication techniques," in *Proc. SPIE*, Moscow, Russia, 2000, vol. 4083, pp. 212–223.

[2] T. Allsop *et al.*, "A comparison and characteristics of sensing parameters of long period gratings written in three different types of fibre," *Opt. Fiber Technol.*, vol. 9, no. 4, pp. 210–223, Oct. 2003.

[3] A. Snyder, "Coupling of modes on a tapered dielectric cylinder," *IEEE Trans. Microw. Theory Tech.*, vol. MTT-18, no. 7, pp. 383–392, Jul. 1970.

[4] S. Rabbany *et al.*, "Optical immunosensor," *Crit. Rev. Biomed. Eng.*, vol. 22, no. 5/6, pp. 307–346, 1994.

[5] F. L. Arregui *et al.*, "Optical fibre strain gauge based a tapered single-mode fibre," *Sens. Actuators A, Phys.*, vol. 79, no. 2, pp. 90–96, Feb. 2000.

[6] H. J. Patrick, "Analysis of the response of long period fiber gratings to external index of refraction," *J. Lightw. Technol.*, vol. 16, no. 9, pp. 1606–1612, Sep. 1998.

[7] T. Allsop *et al.*, "Detection of organic aromatic compounds in paraffin by a long period fibre grating optical sensor with optimised sensitivity," *Opt. Commun.*, vol. 191, no. 3–6, pp. 181–190, May 2001.

[8] ——, "Refractive index sensing with a long period grating fabricated in a biconical tapered fibre," *Electron. Lett.*, vol. 41, no. 8, pp. 471–472, Apr. 2005.

[9] J.-F. Ding *et al.*, "Fiber-taper seeded long-period grating pair as a highly sensitive refractive-index sensor," *IEEE Photon. Technol. Lett.*, vol. 17, no. 6, pp. 1247–1249, Jun. 2005.

[10] A. W. Synder, *Optical Waveguide Theory*. London, U.K.: Chapman and Hall, 1991.

[11] R. J. Black *et al.*, "Core-mode cutoff for finite-cladding lightguides," *Proc. Inst. Elect. Eng.*, vol. J-133, no. 6, pp. 377–384, 1986.

[12] J. D. Love *et al.*, "Tapered single-mode fibres and devices—Part 1: Adiabaticity criteria," *Proc. Inst. Elect. Eng. J*, vol. 133, no. 6, pt. J, pp. 377–384, 1986.

[13] T. Erdogan, "Cladding-mode resonances in short- and long-period fibre grating filters," *J. Opt. Soc. Amer. A, Opt. Image Sci.*, vol. 14, no. 8, pp. 1760–1773, Aug. 1997.

[14] C. Tsao, *Optical Fibre Waveguide Analysis*. New York: Oxford Univ. Press, 1992.

[15] Y. Takeuchi *et al.*, "Novel fiber coupler tapering process using a micro-heater," *IEEE Photon Technol. Lett.*, vol. 4, no. 5, pp. 465–467, May 1992.

[16] R. P. Kenny *et al.*, "Control of optical fibre taper shape," *Electron. Lett.*, vol. 27, no. 18, pp. 1654–1656, Aug. 1991.

[17] D. Marcuse, "Mode conversion in optical fibres with monotonically increasing core radius," *J. Lightw. Technol.*, vol. LT-5, no. 1, pp. 125–133, Jan. 1987.

[18] M. Miyagi *et al.*, "An approximate formula for describing dispersion properties of optical dielectric slab and fibre waveguides," *J. Opt. Soc. Amer. A, Opt. Image Sci.*, vol. 69, no. 2, pp. 291–293, 1979.

[19] T. Allsop *et al.*, "High sensitivity refractometer based upon a long period grating Mach–Zehnder interferometer," *Rev. Sci. Instrum.*, vol. 73, no. 4, pp. 1702–1705, Apr. 2002.

[20] K. Schroeder *et al.*, "A fibre Bragg grating refractometer," *Meas. Sci. Technol.*, vol. 12, no. 7, pp. 757–764, 2001.

T. Allsop, photograph and biography not available at the time of publication.

F. Floreani, photograph and biography not available at the time of publication.

K. P. Jedrzejewski, photograph and biography not available at the time of publication.

P. V. S. Marques, photograph and biography not available at the time of publication.

R. Romero, photograph and biography not available at the time of publication.

D. J. Webb (M'01), photograph and biography not available at the time of publication.

I. Bennion, photograph and biography not available at the time of publication.